Sidewall Morphology-Dependent Formation of Multiple Twins in Si Nanowires

Naechul Shin,[†] Miaofang Chi,[‡] and Michael A. Filler[†,*]

[†]School of Chemical & Biomolecular Engineering, Georgia Institute of Technology, Atlanta, Georgia, 30332, United States and [‡]Materials Science and Technology Division, Oak Ridge National Laboratory, Oak Ridge, Tennessee, 37831, United States

ABSTRACT Precise placement of twin boundaries and stacking faults promises new opportunities to fundamentally manipulate the optical, electrical, and thermal properties of semiconductor nanowires. Here we report on the appearance of consecutive twin boundaries in Si nanowires and show that sidewall morphology governs their spacing. Detailed electron microscopy analysis reveals that thin {111} sidewall facets, which elongate following the first twin boundary (TB_1), are responsible for deforming the triple-phase line and favoring the formation of the second twin boundary (TB_2). While multiple, geometrically correlated defect planes are known in group III–V nanowires, our findings show that this behavior is also possible in group IV materials.

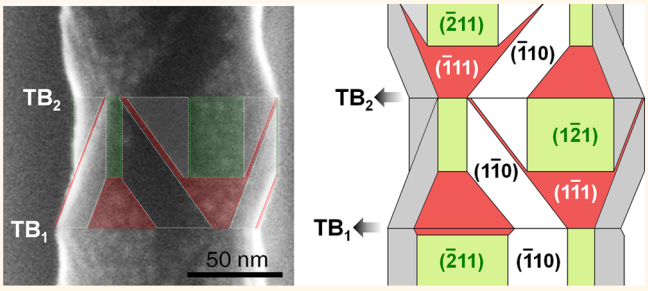

KEYWORDS: silicon · nanowire · defects · twin · surface · facet

The manipulation of semiconductor nanowire properties is possible *via* control of crystal phase,[1] growth orientation,[2] and sidewall faceting,[3] among others.[4,5] Engineering of the bilayer stacking sequence is particularly intriguing, assuming a sufficient level of precision is ultimately achievable, as it offers direct access to a material's optoelectronic and phononic behavior.[6–8] To this end, twin boundaries (TBs) and stacking faults (SFs) have been extensively studied in group III–V nanowires synthesized *via* the vapor–liquid–solid (VLS) method.[9–11] Careful selection of process conditions and dopants now enables periodic sequences of TBs known as twinning superlattices.[12,13]

The frequency and morphology of defects in group IV nanowires, particularly Si, exhibit a number of well-known differences relative to their III–V counterparts. Longitudinal defects, those oriented parallel to the nanowire growth direction, are common in ⟨112⟩ oriented Si nanowires catalyzed by Au.[14–16] Catalysts other than Au (*e.g.*, Cu, Ga, Au/Ag) are also known to randomly generate transverse TBs, those oriented perpendicular to the nanowire growth direction, in ⟨111⟩ oriented Si nanowires.[17–19] We recently reported that the rapid modulation of precursor pressure and substrate temperature can introduce transverse TBs in Au-catalyzed Si nanowires.[20]

Here, we show that two transverse TBs, which exhibit a sidewall morphology-dependent spacing, are possible in ⟨111⟩ oriented Si nanowires. We find, similar to our prior work,[20] that the first TB appears upon raising the Si_2H_6 pressure and reducing the substrate temperature. When maintaining these new conditions for an extended period of time, a second TB sometimes appears at a geometry-dependent distance from the first. A detailed investigation of nanowire morphology reveals that the second TB is coincident with the appearance of thin {111} facets that propagate across the nanowire's {110} sidewall. Algra *et al.* reported on the presence of similar "twin pairs" in III–V nanowires,[21] but the situation in Si nanowires exhibits a number of important differences.

RESULTS AND DISCUSSION

Figure 1a shows representative scanning electron microscopy (SEM) images of

* Address correspondence to michael.filler@chbe.gatech.edu.

Received for review July 17, 2013 and accepted August 14, 2013.

Published online August 14, 2013
10.1021/nn4036798

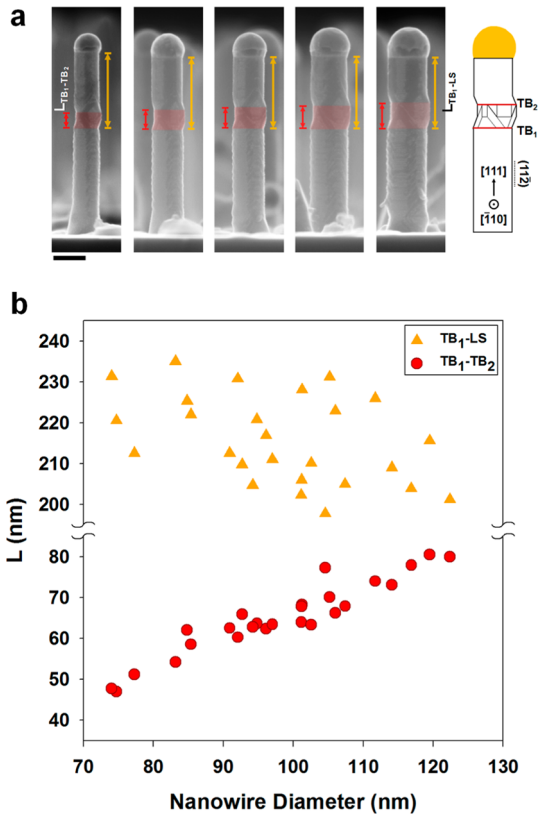

Figure 1. (a) Side view SEM images of representative Si nanowires with a range of diameters measured along the ⟨110⟩ direction that show changes to sidewall morphology near double TBs. A schematic projection of a nanowire containing double TBs onto the ($\bar{1}$10) plane is included for comparison purposes. $L_{TB_1-TB_2}$ is indicated by red lines and defined as the distance between the first (TB_1) and the second (TB_2) TB. The distance between TB_1 and the catalyst−nanowire interface is defined as L_{TB_1-LS} and indicated with orange lines. Scale bar, 100 nm. (b) The values of $L_{TB_1-TB_2}$ and L_{TB_1-LS}, as determined from SEM images of 26 nanowires containing double TBs, plotted as a function of nanowire diameter.

⟨111⟩ oriented Si nanowires containing double TBs, which appear upon increasing the Si_2H_6 pressure from 2×10^{-4} to 5×10^{-4} Torr and lowering the substrate temperature from 490 to 410 °C. The new process conditions are applied after 10 min of initial elongation and maintained for another 10 min. While nanowire diameter ranges from 70 to 130 nm, the growth rate is diameter independent.[22] As the nanowires are imaged along the ⟨110⟩ direction, the characteristic sawtooth faceting of the {112} sidewalls[23] is visible on the left side of each nanowire and provides an initial indication of the first TB's position (denoted TB_1).[20] We note that the axial position of TB_1 is similar for all nanowires and independent of diameter, which indicates that it formed upon changing process conditions.[20] While maintaining the conditions at 5×10^{-4} Torr and 410 °C, a second TB (denoted TB_2) can also appear at some axial distance after TB_1. We identified 161 and 26 nanowires containing single (*i.e.*, TB_1 only) and double TBs (*i.e.*, TB_1 and TB_2), respectively, from a total of 1055 examined nanowires. Thus, the probability of TB_2 appearing after TB_1 is 13.9%. While this probability is clearly low, and not yet appropriate, for defect superstructure engineering, the geometric relationship described herein provides important insight into the defect introduction mechanism in Si nanowires.

The distance between TB_1 and the liquid−solid (*i.e.*, catalyst−nanowire) interface, defined as L_{TB_1-LS} and shown as orange lines in Figure 1a, is plotted as a function of nanowire diameter in Figure 1b. Since TB_1 forms upon raising Si_2H_6 pressure and lowering substrate temperature,[20] L_{TB_1-LS} represents the portion of the nanowire grown after the condition change and, as is evident from the plot, the growth rate (~22 nm/min) remains largely diameter-independent over this length. We also define $L_{TB_1-TB_2}$, indicated by the red lines in Figure 1a, as the distance between TB_1 and TB_2. Figure 1b shows $L_{TB_1-TB_2}$ plotted as a function nanowire diameter and reveals a clear diameter-dependence. TB_2 nucleates earlier in nanowires with small diameters and later in nanowires with large diameters. Since the process conditions are fixed following TB_1, the observed diameter-dependence of TB_2 position suggests that it forms due to a geometric effect. We return to this point below.

High-resolution transmission electron microscopy (HRTEM) images, measured along the ⟨110⟩ zone axis of a representative Si nanowire with a double TB are displayed in Figure 2. Figure 2a shows the change of overall sidewall morphology for both TBs. Corresponding Fast Fourier Transforms (FFTs) confirm that the crystal structure rotates by 180° about the ⟨111⟩ axis at each TB (Supporting Information, Figure S1). The evolution of catalyst contact angle near each TB is also consistent with double TB formation (Supporting Information, Figure S2). The aberration-corrected high angle annular dark field scanning transmission electron microscopy (HAADF-STEM) images shown in Figure 2c,f verify that TB_1 and TB_2 are composed of single twin planes, unlike the defect arrays frequently observed in ⟨112⟩ oriented Si nanowires.[24−26]

Figure 2b,d,e,g reveals the detailed sidewall morphology before and after each TB. Immediately prior to TB_1 and consistent with our previous report,[20] inward moving {111} facets emerge from the broad {112} sidewall (Figure 2g), but the narrow, sawtooth faceted {112} facet on the opposite sidewall is not significantly impacted (Figure 2e). After TB_1, six {111} sidewalls emerge from the original {112} sidewalls.[20] Conversely, and importantly, TB_2 forms without the formation of inward moving {111} facets on the broad {112} sidewall (Figure 2b). As the process conditions remained constant since the formation of TB_1, this result implies that the mechanism underlying TB_2 formation is distinct from that for TB_1. However, and similar to TB_1, six {111} facets appear immediately after TB_2. We also note that the six {111} facets appearing following TB_1

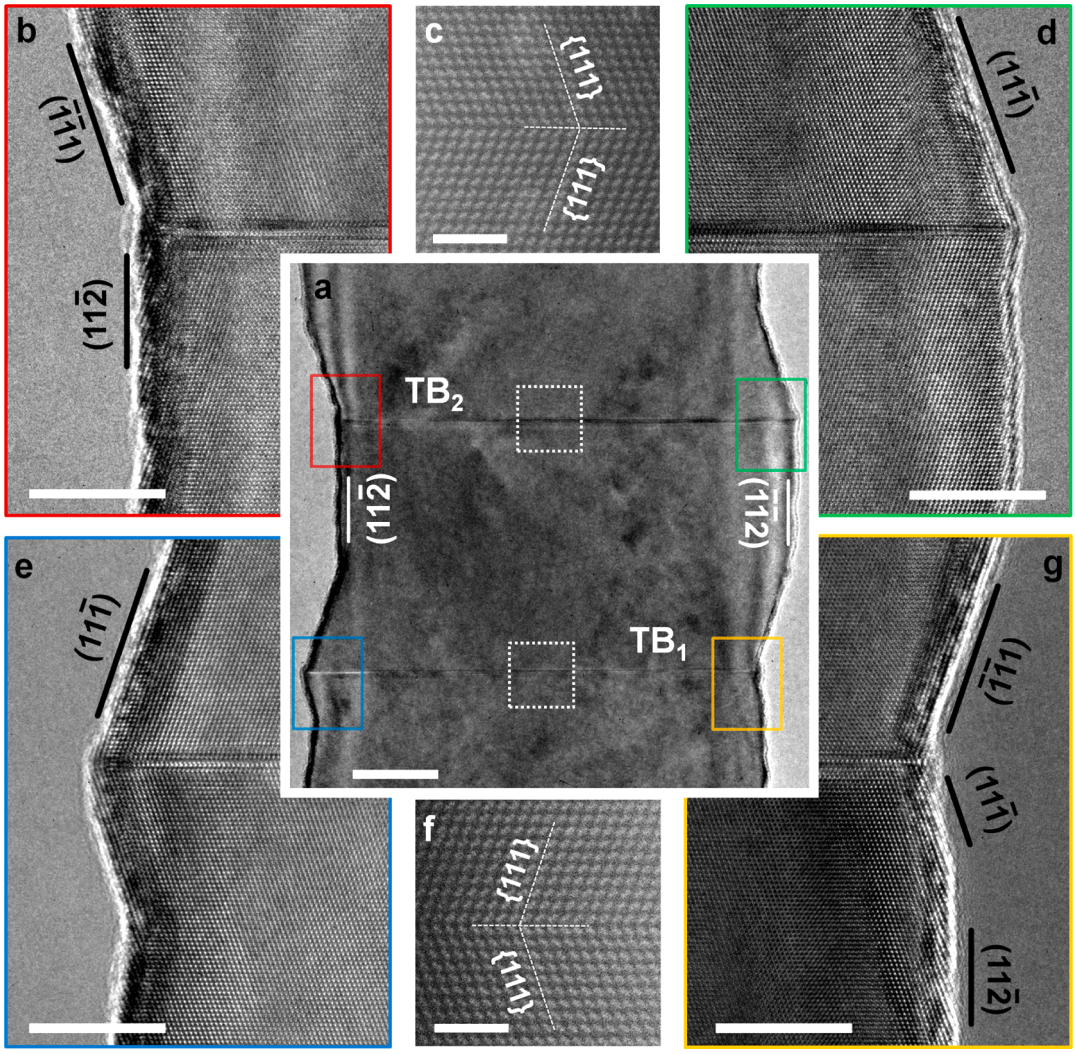

Figure 2. Representative TEM images of the region near double TBs in Si nanowires measured along the [$\bar{1}$10] zone axis. (a) Low-magnification bright field image showing the overall structure of a double TB. Scale bar, 20 nm. High resolution bright field images of (b, d) TB_2 and (e, g) TB_1 in the regions denoted by the boxes in (a). Scale bars, 10 nm. (c, f) Aberration-corrected HAADF-STEM images of (c) TB_2 and (f) TB_1 measured in the regions denoted by the dotted white boxes in (a). Scale bars, 2 nm.

and TB_2 eventually revert to {112} facets (Figure 2a). Although {110} facets cannot be identified when the nanowire is viewed along this zone axis, they are present before and after each TB (*vida infra*).

A careful analysis of SEM images taken along the ⟨112⟩ and ⟨110⟩ directions for representative nanowires containing single and double TBs, as shown in Figure 3, provides additional information regarding the evolution of the sidewall morphology in the vicinity of TB_1 and TB_2. Due to the complexity of the sidewall morphology, illustrations that schematically show each facet are also included with each SEM image. {112}, {111}, and {110} facets are colored in green, red, and white, respectively. While all nanowires exhibit six {112} sidewalls separated by {110} facets prior to TB_1, as is well documented for Si nanowires under similar growth conditions,[27,28] we subsequently observe important morphological differences for single and double TBs. When viewing nanowires containing single and double TBs along the ⟨112⟩ direction (Figure 3a,b), the left and right sidewalls appear perpendicular to the ⟨111⟩ growth direction, which indicates that these are {110} facets. Upon rotating the nanowire to the ⟨110⟩ viewing direction (Figure 3c,d), it can be seen that these {110} planes, which appear dark as a result of reduced Au wetting,[28] propagate at an angle across the nanowire sidewall. SEM images measured at a range of angles relative to the substrate normal indicate that these {110} sidewalls are nearly in the same plane before and after TB_1 and TB_2 (Supporting Information, Figure S3). When viewing both types of nanowire along the ⟨110⟩ direction (Figure 3c,d), and *via* comparison with the TEM images in Figure 2, large {111} facets that separate the {110} facets are identifiable after each TB.

The sidewalls of nanowires that contain single and double TBs exhibit a number of key differences above TB_1. In the case of single TBs, the {111} facets revert to

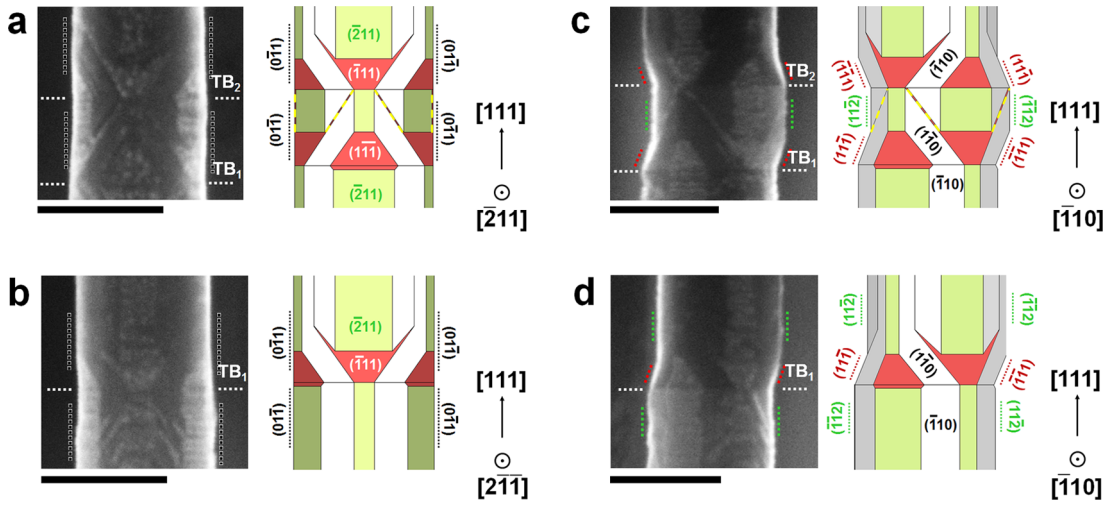

Figure 3. Side view SEM images and schematic illustrations of the sidewall morphology for representative single and double TBs in Si nanowires. (a) Double and (b) single TBs viewed along the ⟨112⟩ direction. (c) Double and (d) single TBs viewed along the ⟨110⟩ direction. In each SEM image, the location of TBs as well as key {112}, {111}, and {110} facets are denoted by the white, green, red, and black dotted lines, respectively. In the schematics, {112}, {111}, and {110} facets are labeled as such and shaded in green, red, and white, respectively. The thin {111} facets present for double TBs are shown as yellow dashed lines. Scale bars, 100 nm.

{112} orientation at some distance beyond TB_1 and the sidewall morphology matches that prior to changing process conditions, albeit rotated by 180° (Figure 3d). For double TBs, very thin, diagonally oriented facets, which are identified by the bright lines observed in the SEM image and represented by dashed yellow lines in the Figure 3a,c schematics, are visible before TB_2. These facets are assigned to {111} because they extend from the edge between {110} and {111} facets and continue even though the majority of the {111} facets reverts to {112}. Angle-dependent SEM images provide another view of these facets (Supporting Information, Figure S3). Pairs of these thin {111} facets propagate toward each other across {110} facets until they intersect the {110}/{112} edge near TB_2. While the same, thin {111} facets initially appear for some nanowires containing single TBs, they terminate much earlier (Figure 3b,d). Double TBs can also exhibit thin {111} facets after TB_2 that disappear in the same manner as those for nanowires with a single TB.

We propose a mechanism, as illustrated in Figure 4, for double TB formation based on the above-described changes in sidewall morphology. As we reported previously,[20] TB_1 formation appears due to the increase in Si_2H_6 pressure and decrease in substrate temperature. The triple-phase line (*i.e.*, where the vapor, liquid, and solid meet) becomes increasing triangular due to the three new, inward propagating {111} facets and TB_1 eventually nucleates to reduce the line tension (Figure 4a). The sidewall morphology continues to evolve under the new Si_2H_6 pressure and substrate temperature after TB_1. Of the six {111} facets that appear immediately following TB_1, the width of all inward moving {111} facets, $(\bar{1}11)$, $(1\bar{1}1)$, and $(11\bar{1})$, increases, while the width of the outward moving {111} facets, $(\bar{1}1\bar{1})$, $(\bar{1}\bar{1}1)$, and $(1\bar{1}\bar{1})$, decreases. {110} facets, which are also present and separate the {111} planes, maintain their width as the nanowire elongates.

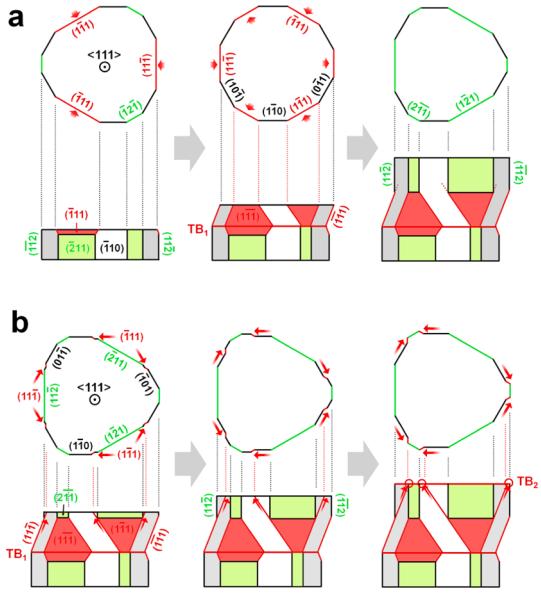

Figure 4. Schematic illustrations of (a) single and (b) double TB formation during Si nanowire elongation. In all illustrations, {112}, {111}, and {110} facets are labeled as such and shaded in green, red, and white, respectively. Red arrows indicate the direction of facet propagation. In the case of single TBs, deformation of the triple-phase line occurs following the formation of inward moving {111} facets after the increase of Si_2H_6 pressure and decrease of substrate temperature. After TB_1, {111} facets continue until the {112} sidewalls remerge. In the case of double TBs, thin {111} facets, highlighted by red arrows, survive after the {112} sidewalls reappear and propagate diagonally across the {110} facet. {111} facet propagation beyond the opposite {110}/{112} edge is highly unfavorable and TB_2 nucleates to reduce the triple-phase line tension. Thin {111} facets, shown as short dotted red lines in (a), occasionally appear following the reappearance of {112} sidewalls for the case of single TBs, but disappear before reaching the opposite {110}/{112} edge.

For most of the nanowires in our study, the entire {111} facet reverts to {112} at some distance beyond TB_1 and no second TB (*i.e.*, TB_2) is observed. However, nanowires with two TBs exhibit thin {111} facets, which continue to propagate across the {110} facet even after the reversion to {112} (Figure 4b). These thin {111} facets eventually reach the {110}/{112} edge at the opposite side of the {110} facet. Beyond this point, the facets cannot extend without protruding from the nanowire sidewall and TB nucleation becomes favored over further deformation of the triple-phase line. Notably, the {112} sidewall does not undergo any obvious changes during this process (Figure 2b), which indicates that the thin {111} facets are largely responsible for deforming the triple-phase line and generating TB_2.

The above mechanism implies that the continued presence of thin {111} facets may enable some nanowires to contain three or more TBs. While we found a handful of nanowires with triple TBs, no nanowires with four or more TBs were observed (Supporting Information, Figure S4). Nonetheless, nanowires exhibiting triple TBs contained thin {111} facets after TB_1 *and* TB_2, a finding that further supports the proposed mechanism. We expect that process conditions, where six {111} facets appear after each TB, but do not revert to {112}, will lead to a more dramatic deformation of the triple-phase line, generation of more closely spaced TBs and, ultimately, the appearance of twinning superlattices.[12,13]

Additional evidence that the thin {111} facets underlie TB_2 nucleation comes from a correlation of {110} facet width with the distance between TB_1 and TB_2 ($L_{TB_1-TB_2}$). More specifically, the thin {111} facets must propagate across the {110} facet before deforming the triple-phase line to the point where TB_2 forms and, as such, we expect the width of this facet to be linearly related to $L_{TB_1-TB_2}$. Two important length scales, specifically l_1 and l_2, are identified in Figure 5a and sum to give $L_{TB_1-TB_2}$. l_1 is the axial length between TB_1 and the point where the majority of {111} sidewall reverts to {112}. As illustrated in Figure 4, six {111} and six {110} sidewalls bound the nanowire over this length. l_2 is the axial distance from the point where the {112} sidewalls reappear to TB_2. Over this length, the nanowires containing double TBs are bounded by six {112} and six {110} surfaces, as well as the thin {111} facets. Figure 5b shows the relationship between l_1 and l_2, as measured from high resolution SEM images, and nanowire diameter. These data clearly show that l_1 and l_2 are linearly related to diameter, with the l_2 dependence being stronger. Because $L_{TB_1-TB_2}$ is simply the sum of l_1 and l_2, the linear dependence of $L_{TB_1-TB_2}$ with nanowire diameter (Figure 1b) arises primarily from changes in l_2.

A projection of the nanowire onto the $(1\bar{1}0)$ plane in the region between TB_1 and TB_2 is schematically illustrated in Figure 6a, where the actual ($w_{\{110\}}$) and

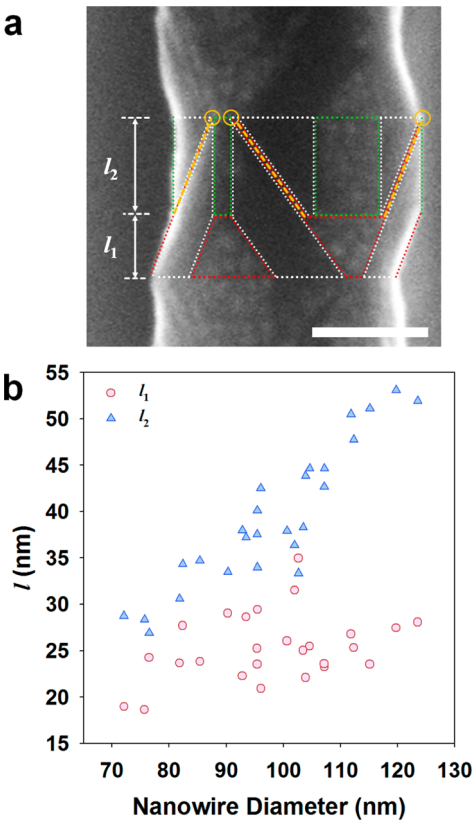

Figure 5. Correlation of TB spacing with sidewall morphology. (a) Side view SEM image of a representative Si nanowire containing a double TB. The {112}, {111}, and {110} facets are delineated by green, red, and white dashed lines, respectively. The thin {111} facets, which propagate across the {110} facet, are shown as dashed yellow lines, and the point where they intersect the opposite {110}/{112} edge is circled in yellow. The axial distance between TB_1 and the point where the {112} sidewalls reemerge is defined as l_1, while l_2 is the axial distance between the point where the {112} sidewalls reappear and TB_2. Scale bar, 50 nm. (b) l_1 and l_2 measured from SEM images of the same 26 nanowires used in Figure 1b plotted as function of nanowire diameter.

apparent ($w_{\{110\}}'$ and $w_{\{111\}}'$) facet widths are labeled. While $w_{\{110\}}$ can be directly measured when viewing the nanowire along the ⟨110⟩ direction, $w_{\{111\}}$ must be indirectly determined. Thus, we measure $w_{\{111\}}'$ and then convert this value to $w_{\{111\}}$ by knowing the angle between {110} and {111} facets is 30°:

$$w_{\{111\}} = \frac{w_{\{111\}}'}{\cos(30°)} = \frac{2}{\sqrt{3}} w_{\{111\}}' \qquad (1)$$

Based on high-resolution SEM images and the above relationship, the values of $w_{\{110\}}$ and $w_{\{111\}}$ were extracted (Supporting Information, Figure S5). While both $w_{\{110\}}$ and $w_{\{111\}}$ are linearly correlated with diameter, the dependence of $w_{\{110\}}$ is much stronger and less variable than $w_{\{111\}}$.

The values of l_1 and l_2 are now plotted as a function of $w_{\{111\}}$ and $w_{\{110\}}$, respectively, in Figure 6b. While the data points are extracted from experiment, it is important to note that the lines are not fits to these data and we discuss their origin below. We see that l_2

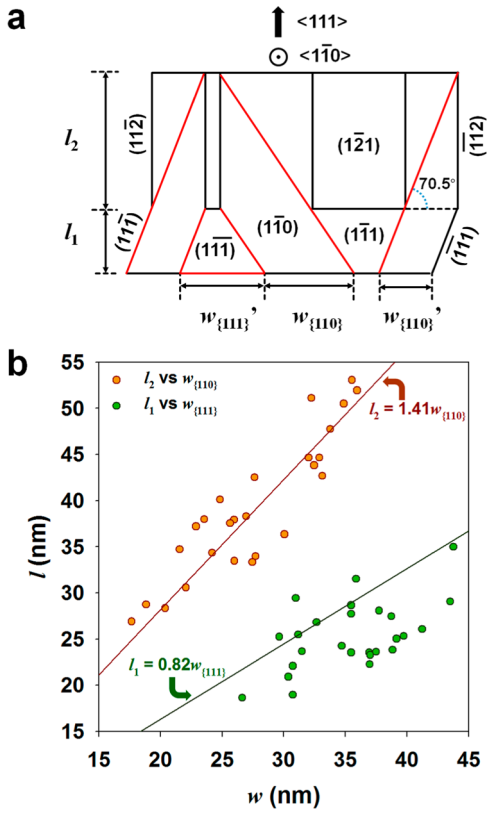

Figure 6. (a) Schematic illustration showing the projection of a Si nanowire containing a double TB onto the (1$\bar{1}$0) plane. $w_{\{111\}}$ and $w_{\{111\}}'$ are defined as the actual and apparent widths, respectively, of the large {111} facets. $w_{\{110\}}$ and $w_{\{110\}}'$ are defined as the actual and apparent widths, respectively, of the {110} facets. (b) l_1 and l_2 plotted as a function of $w_{\{111\}}$ and $w_{\{110\}}$, respectively. Data points are experimentally derived from measurements of SEM images. Solid lines are plots of the equations relating l_1/l_2 and $w_{\{111\}}/w_{\{110\}}$, specifically $l_1 = 0.82w_{\{111\}}$ and $l_2 = 1.41w_{\{110\}}$, as derived from the nanowire structure shown in (a).

depends linearly on $w_{\{110\}}$, and because the value of l_2 is largely responsible for the change of $L_{TB_1-TB_2}$, we then know that $w_{\{110\}}$ also correlates with $L_{TB_1-TB_2}$. In other words, as {110} facet width increases, so too does the distance between TB_1 and TB_2. This finding is consistent with the proposed mechanism, whereby thin {111} facets propagate across the {110} plane and, in doing so, deform the triple phase line. As the {110} facet width increases (*i.e.*, for larger diameter nanowires), the distance that these thin {111} facets must travel before reaching the opposite {112}/{110} edge also increases. This additional length requires that the nanowire elongate further before TB_2 nucleates.

We now compare our proposed model of nanowire sidewall evolution (*i.e.*, Figure 4) and final morphology (*i.e.*, Figure 3 and 6a) with parameters extracted from experiment (*i.e.*, l_1, l_2, $w_{\{111\}}$, and $w_{\{110\}}$). This comparison serves to further validate the structure derived from our electron microscopy measurements and is particularly valuable due to the complexity seen here. If the 6 {111} facets present over the length l_1 comprise the surfaces of an ideal octahedron,[9] the relationship between $w_{\{111\}}$ and l_1 would be

$$l_1 = \frac{w_{\{111\}}}{2} \times \tan(60°) \times \sin(70.5°)$$
$$= 0.82w_{\{111\}} \quad (2)$$

We can determine the relationship between $w_{\{110\}}$ and l_2 similarly. If the {110} facet width is constant, as the nanowire cross-section evolves over the length l_1, as indicated by our data (Figure 3c and 5a), the projection of the nanowire in the (1$\bar{1}$0) plane (Figure 6a) allows us to relate l_2 and $w_{\{110\}}'$ (*i.e.*, the apparent width of the {110} facet) as follows:

$$l_2 = w_{\{110\}}' \times \tan(70.5°) \quad (3)$$

The value of $w_{\{110\}}'$ can be related to $w_{\{110\}}$ (*i.e.*, the actual width of the {110} facet) because all {110} sidewalls are oriented 60° relative to each other:

$$w_{\{110\}}' = w_{\{110\}} \times \cos(60°) = \frac{w_{\{110\}}}{2} \quad (4)$$

By combining eqs 3 and 4, we find that

$$l_2 = w_{\{110\}}' \times \tan(70.5°) = \frac{w_{\{110\}} \times \tan(70.5°)}{2}$$
$$= 1.41w_{\{110\}} \quad (5)$$

Eqs 2 and 5 indicate that l_1 and l_2 are directly proportional to the width of {111} and {110} facets, respectively. Inclusion of the lines described by these equations (Figure 6b), which are based on the structural model alone (Figure 6a), shows excellent agreement with our experimental measurements. The clear correspondence strongly supports the validity of the proposed sidewall structure and double TB formation mechanism. We note that the values measured for l_1 are less than predicted by the structural model, and we suspect that this stems from our assumption that the nanowire is an ideal octahedron over the length l_1. In reality, our images indicate that the octahedron is slightly truncated (Figure 5a), a result that would overestimate the value of l_1.

CONCLUSION

We demonstrate that multiple transverse TBs are possible in ⟨111⟩ oriented Si nanowires and that sidewall morphology controls their spacing. While the first TB (TB_1) is driven by inward moving {111} facets that form following an abrupt increase in Si_2H_6 pressure and decrease of substrate temperature, another TB (TB_2) results from a different set of thin {111} facets that traverse the {110} sidewalls. Both mechanisms, while distinct in their details, deform the triple-phase line and eventually favor TB nucleation. Detailed measurements of the sidewall show that {110} facet width governs TB_2 position and support the proposed model

of nanowire morphology. It remains to be determined why the efficiency of TB_1 and TB_2 introduction is low. We recently suggested that local differences in triple-phase line shape, as a result of asynchronous sawtooth faceting, reduce the probability of TB_1 formation.[20] In terms of TB_2, the observed reversion of {111} facets to {112} suggests that the energetics of these two surfaces are similar under our growth conditions. As such, we anticipate that the further stabilization of {111} facets (*i.e.*, relative to {112}), possibly *via* surface functionalization or modification of catalyst droplet composition, will enable the fabrication of periodic defect superstructures similar to those seen in III–V nanowires.

METHODS

Si nanowires were prepared in a custom built ultrahigh vacuum (UHV) chamber with a base pressure of 3×10^{-10} Torr.[16] Nanowire growth begins with an incubation step, where a flash-annealed Si (111) substrate covered with a 2 nm Au film is ramped to 590 °C and exposed to 2×10^{-4} Torr Si_2H_6 (Voltaix, 99.998%) for 2 min. The substrate temperature is subsequently lowered to 490 °C at a rate of 3 °C/s while maintaining a constant Si_2H_6 pressure. After 10 min of elongation at 490 °C and 2×10^{-4} Torr Si_2H_6, the Si_2H_6 pressure is increased to 5×10^{-4} Torr and substrate temperature decreased to 410 °C at a rate of 8 °C/s. The growth is continued at these conditions for another 10 min. Nanowire sidewall morphologies are analyzed *via* a Zeiss Ultra 60 field emission scanning electron microscope (SEM). High resolution bright field transmission electron microscopy (TEM) and aberration-corrected high angle annular dark field scanning transmission electron microscopy (HAADF-STEM) images are obtained with a FEI Titan S 80–300 microscope. Samples for TEM analysis are prepared *via* substrate ultrasonication in isopropyl alcohol for 15 min and subsequent dispersion of the resulting nanowire suspension onto lacey carbon grids (Ted Pella).

Conflict of Interest: The authors declare no competing financial interest.

Acknowledgment. The authors acknowledge funding from the National Science Foundation (CBET# 1133563) and greatly appreciate insightful comments from Karren More. Research supported by ORNL's Shared Research Equipment (ShaRE) User Program, which is sponsored by the Office of Basic Energy Sciences, the U.S. Department of Energy.

Supporting Information Available: FFT images showing the crystal orientation change at each TB; post-growth SEM images of catalyst contact angle measurements; angle-dependent SEM images of nanowires containing double TBs; examples of nanowires containing triple TBs; correlation of $w_{\{111\}}$ and $w_{\{110\}}$ with nanowire diameter. This material is available free of charge *via* the Internet at http://pubs.acs.org.

REFERENCES AND NOTES

1. Akopian, N.; Patriarche, G.; Liu, L.; Harmand, J. C.; Zwiller, V. Crystal Phase Quantum Dots. *Nano Lett.* **2010**, *10*, 1198–1201.
2. Tian, B. Z.; Xie, P.; Kempa, T. J.; Bell, D. C.; Lieber, C. M. Single-Crystalline Kinked Semiconductor Nanowire Superstructures. *Nat. Nanotechnol.* **2009**, *4*, 824–829.
3. Hochbaum, A. I.; Chen, R. K.; Delgado, R. D.; Liang, W. J.; Garnett, E. C.; Najarian, M.; Majumdar, A.; Yang, P. D. Enhanced Thermoelectric Performance of Rough Silicon Nanowires. *Nature* **2008**, *451*, 163–167.
4. Xie, P.; Hu, Y. J.; Fang, Y.; Huang, J. L.; Lieber, C. M. Diameter-Dependent Dopant Location in Silicon and Germanium Nanowires. *Proc. Natl. Acad. Sci. U.S.A.* **2009**, *106*, 15254–15258.
5. Zhang, G. Q.; Wang, W.; Li, X. Enhanced Thermoelectric Properties of Core/Shell Heterostructure Nanowire Composites. *Adv. Mater.* **2008**, *20*, 3654–3656.
6. Perera, S.; Pemasiri, K.; Fickenscher, M. A.; Jackson, H. E.; Smith, L. M.; Yarrison-Rice, J.; Paiman, S.; Gao, Q.; Tan, H. H.; Jagadish, C. Probing Valence Band Structure in Wurtzite InP Nanowires Using Excitation Spectroscopy. *Appl. Phys. Lett.* **2010**, *97*, 023106.
7. Ketterer, B.; Heiss, M.; Uccelli, E.; Arbiol, J.; Fontcuberta i Morral, A. Untangling the Electronic Band Structure of Wurtzite GaAs Nanowires by Resonant Raman Spectroscopy. *ACS Nano* **2011**, *5*, 7585–7592.
8. Assali, S.; Zardo, I.; Plissard, S.; Kriegner, D.; Verheijen, M. A.; Bauer, G.; Meijerink, A.; Belabbes, A.; Bechstedt, F.; Haverkort, J. E. M.; et al. Direct Band Gap Wurtzite Gallium Phosphide Nanowires. *Nano Lett.* **2013**, *13*, 1559–1563.
9. Johansson, J.; Karlsson, L. S.; Svensson, C. P. T.; Martensson, T.; Wacaser, B. A.; Deppert, K.; Samuelson, L.; Seifert, W. Structural Properties of ⟨111⟩ B-Oriented III–V Nanowires. *Nat. Mater.* **2006**, *5*, 574–580.
10. Xiong, Q.; Wang, J.; Eklund, P. C. Coherent Twinning Phenomena: Towards Twinning Superlattices in III–V Semiconducting Nanowires. *Nano Lett.* **2006**, *6*, 2736–2742.
11. Verheijen, M. A.; Algra, R. E.; Borgstrom, M. T.; Immink, G.; Sourty, E.; van Enckevort, W. J. P.; Vlieg, E.; Bakkers, E. P. A. M. Three-Dimensional Morphology of GaP-GaAs Nanowires Revealed by Transmission Electron Microscopy Tomography. *Nano Lett.* **2007**, *7*, 3051–3055.
12. Algra, R. E.; Verheijen, M. A.; Borgstrom, M. T.; Feiner, L.-F.; Immink, G.; van Enckevort, W. J. P.; Vlieg, E.; Bakkers, E. P. A. M. Twinning Superlattices in Indium Phosphide Nanowires. *Nature* **2008**, *456*, 369–372.
13. Caroff, P.; Dick, K. A.; Johansson, J.; Messing, M. E.; Deppert, K.; Samuelson, L. Controlled Polytypic and Twin-Plane Superlattices in III–V Nanowires. *Nat. Nanotechnol.* **2009**, *4*, 50–55.
14. Carim, A. H.; Lew, K. K.; Redwing, J. M. Bicrystalline Silicon Nanowires. *Adv. Mater.* **2001**, *13*, 1489–1491.
15. Dayeh, S. A.; Wang, J.; Li, N.; Huang, J. Y.; Gin, A. V.; Picraux, S. T. Growth, Defect Formation, and Morphology Control of Germanium-Silicon Semiconductor Nanowire Heterostructures. *Nano Lett.* **2011**, *11*, 4200–4206.
16. Shin, N.; Filler, M. A. Controlling Silicon Nanowire Growth Direction *via* Surface Chemistry. *Nano Lett.* **2012**, *12*, 2865–2870.
17. Arbiol, J.; Fontcuberta i Morral, A.; Estrade, S.; Peiro, F.; Kalache, B.; Roca i Cabarrocas, P.; Ramon Morante, J. Influence of the (111) Twinning on the Formation of Diamond Cubic/Diamond Hexagonal Heterostructures in Cu-Catalyzed Si Nanowires. *J. Appl. Phys.* **2008**, *104*, 064312.
18. Conesa-Boj, S.; Zardo, I.; Estrade, S.; Wei, L.; Alet, P. J.; Roca i Cabarrocas, P.; Morante, J. R.; Peiro, F.; Fontcuberta i Morral, A.; Arbiol, J. Defect Formation in Ga-Catalyzed Silicon Nanowires. *Cryst. Growth Des.* **2010**, *10*, 1534–1543.
19. Chou, Y.-C.; Wen, C.-Y.; Reuter, M. C.; Su, D.; Stach, E. A.; Ross, F. M. Controlling the Growth of Si/Ge Nanowires and Heterojunctions Using Silver–Gold Alloy Catalysts. *ACS Nano* **2012**, *6*, 6407–6415.
20. Shin, N.; Chi, M.; Howe, J. Y.; Filler, M. A. Rational Defect Introduction in Silicon Nanowires. *Nano Lett.* **2013**, *13*, 1928–1933.
21. Algra, R. E.; Verheijen, M. A.; Feiner, L.-F.; Immink, G. G. W.; Theissmann, R.; van Enckevort, W. J. P.; Vlieg, E.; Bakkers, E. P. A. M. Paired Twins and {11$\bar{2}$} Morphology in GaP Nanowires. *Nano Lett.* **2010**, *10*, 2349–2356.

22. Kodambaka, S.; Tersoff, J.; Reuter, M. C.; Ross, F. M. Diameter-Independent Kinetics in the Vapor−Liquid−Solid Growth of Si Nanowires. *Phys. Rev. Lett.* **2006**, *96*, 096105.
23. Ross, F. M.; Tersoff, J.; Reuter, M. C. Sawtooth Faceting in Silicon Nanowires. *Phys. Rev. Lett.* **2005**, *95*, 146104.
24. Davidson, F. M.; Lee, D. C., III; Fanfair, D. D.; Korgel, B. A. Lamellar Twinning in Semiconductor Nanowires. *J. Phys. Chem. C* **2007**, *111*, 2929–2935.
25. Lopez, F. J.; Givan, U.; Connell, J. G.; Lauhon, L. J. Silicon Nanowire Polytypes: Identification by Raman Spectroscopy, Generation Mechanism, and Misfit Strain in Homostructures. *ACS Nano* **2011**, *5*, 8958–8966.
26. Barth, S.; Boland, J. J.; Holmes, J. D. Defect Transfer from Nanoparticles to Nanowires. *Nano Lett.* **2011**, *11*, 1550–1555.
27. Oehler, F.; Gentile, P.; Baron, T.; Ferret, P.; Den Hertog, M.; Rouviere, J. The Importance of the Radial Growth in the Faceting of Silicon Nanowires. *Nano Lett.* **2010**, *10*, 2335–2341.
28. Boukhicha, R.; Gardes, C.; Vincent, L.; Renard, C.; Yam, V.; Fossard, F.; Patriarche, G.; Jabeen, F.; Bouchier, D. Gold Anchoring on Si Sawtooth Faceted Nanowires. *Europhys. Lett.* **2011**, *95*, 18004.